

# Impact of AC and DC Electric Fields on the Microstructure Evolution in Strontium Titanate

Jan-Helmut Preusker, Michael Johannes Hoffmann, and Wolfgang Rheinheimer\*

Herein, the impact of AC and DC electric fields on microstructure evolution in strontium titanate is investigated. The focus is on nonthermal effects by using current-blocking electrodes. The seeded polycrystal technique allows investigating the impact of a DC electric field on grain growth for different grain-boundary orientations and the impact of the surrounding atmosphere. As in previous studies, faster grain growth is observed at the negative electrode. This effect is stronger for the (100) orientation and in reducing atmosphere. In AC electric field at 1450 °C, a low-enough frequency results in faster grain growth at both electrodes. These findings agree well with previous studies, where an electromigration of oxygen vacancies is found to cause a local reduction at the negative electrode, resulting in less space charge, less cationic segregation, and a higher grain-boundary mobility. At 1500 °C, AC electric fields are found to cause a complete grain growth stagnation at very small grain sizes. This behavior is unexpected; the physical reasons are not clear. Herein, a brief study of sintering in DC electric field reveals slightly faster sintering if a field is applied.

For flash sintering, the observed effects include electromigration and interaction of defects with space-charge zone,<sup>[6–8]</sup> formation of a liquid phase,<sup>[9–11]</sup> or increased cation mobility.<sup>[12]</sup> In addition, other non-thermal field effects such as reduced grain-boundary width for twisted SrTiO<sub>3</sub> bicrystals produced in an electric field by diffusion bonding,<sup>[13–15]</sup> faster densification of yttrium-stabilized zirconia (YSZ) by limiting grain growth during sintering<sup>[16]</sup> or by reducing the activation energy for defect formation,<sup>[17]</sup> faster densification in sodium potassium niobate (KNN) ceramics by a field-assisted formation of a liquid phase,<sup>[18]</sup> or the reduction of grain growth by the interaction of the applied field with the space-charge zone<sup>[19]</sup> have been reported. The direct influence of electric fields on defect generation has been shown to be implausible using CeO<sub>2</sub> as an example,<sup>[20,21]</sup> since an increase in

field-directed diffusion for usually slow cations by five orders of magnitude at 1000 °C would require a field of 10<sup>9</sup> V m<sup>-1</sup>.

Considerable effort aimed on understanding all of the field-assisted processes to harvest the full potential of field-assisted microstructure evolution, such as the generation of phases and microstructures which cannot be produced conventionally.<sup>[22]</sup> One observation in flash sintering was a microstructure gradient from one electrode to the other. This was not always attributed by an inhomogeneous sample temperature, but often by nonthermal effects. One hypothesis is that these microstructure gradients are caused by electromigration and by the interaction of defects with the space-charge zone.<sup>[6–8,20]</sup> Graded microstructures were observed after field-assisted processing of ZnO,<sup>[23,24]</sup> CeO<sub>2</sub>,<sup>[25,26]</sup> Al<sub>2</sub>O<sub>3</sub>,<sup>[9,10]</sup> and TiO<sub>2</sub>,<sup>[27–29]</sup> ZrO<sub>2</sub>,<sup>[30–32]</sup> and SrTiO<sub>3</sub>.<sup>[6–8,33]</sup>

This study focusses on the occurrence of microstructural gradients during field-assisted processing. Previous studies on microstructure evolution in electric field in strontium titanate are reviewed in Section 3. We extend results from earlier studies.<sup>[6–8]</sup> Strontium titanate was chosen as a model system because of its well-known fundamental physics, including the defect chemistry,<sup>[34]</sup> defect migration,<sup>[13,35–40]</sup> space-charge layers,<sup>[41–44]</sup> field-free grain growth data,<sup>[45–52]</sup> and the atomistic grain growth mechanism.<sup>[53–56]</sup> We use the same current-blocking setup as in previous studies (refs. [6,7], **Figure 1**) to shed light on the influence of atmosphere, alternating electric fields and single-crystal orientation on grain growth and densification during field-assisted heat treatments of strontium titanate. The aim of the study is to deepen our understanding of the connection of migrating point defects, the space-charge layer, and grain-boundary migration, allowing for

## 1. Introduction

Field-assisted processes for microstructure development have occupied scientists and engineers for more than three decades.<sup>[1–4]</sup> Still, our mechanistic understanding of the underlying physics is somewhat incomplete. This is particularly true for flash sintering, where multiple processes and physical phenomena occur in parallel, resulting in a challenging situation for scientists.<sup>[5]</sup>

J.-H. Preusker, M. J. Hoffmann  
Karlsruhe Institute of Technology (KIT)  
Institute of Applied Materials – Ceramic Materials and Technologies (IAM-KWT)  
Haid-und-Neu-Str. 7, 76131 Karlsruhe, Germany

W. Rheinheimer  
Forschungszentrum Jülich  
Institute of Energy and Climate Research – Materials Synthesis and Processing (IEK-1)  
52428 Jülich, Germany  
E-mail: w.rheinheimer@fz-juelich.de

 The ORCID identification number(s) for the author(s) of this article can be found under <https://doi.org/10.1002/adem.202201848>.

© 2023 The Authors. Advanced Engineering Materials published by Wiley-VCH GmbH. This is an open access article under the terms of the Creative Commons Attribution-NonCommercial-NoDerivs License, which permits use and distribution in any medium, provided the original work is properly cited, the use is non-commercial and no modifications or adaptations are made.

DOI: 10.1002/adem.202201848

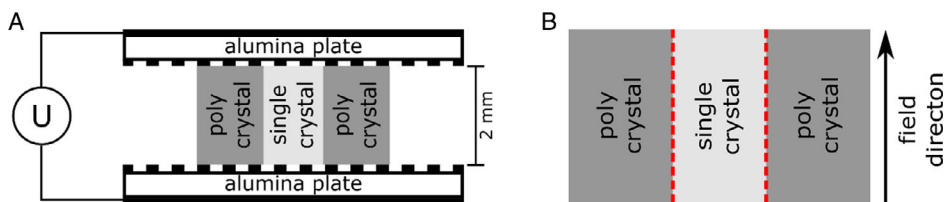


**Figure 1.** A) Experimental setup used in the present study. Platinum electrodes with alumina plates were used to block electric currents. The black dashed line represents a thin layer of coarse zirconia powder to prevent a solid-state reaction between alumina and strontium titanate. B) The microstructures were analyzed by scanning electron microscope (SEM) along the red dashed lines.

an additional parameter to control microstructure evolution, that is, to obtain faster or slower grain growth.

## 2. Experimental Section

Stoichiometric strontium titanate was synthesized with the mixed oxide/carbonate route based on  $\text{SrCO}_3$  and  $\text{TiO}_2$  (both 99.9%, Sigma Aldrich Chemie GmbH, Taufkirchen, Germany). The most important process steps were an initial attrition milling at 1000 rpm for 4 h with 2 mm zirconia balls, a calcination at 975 °C for 3 h and, finally, planetary ball milling at 300 rpm for 16 h with 10 mm zirconia balls. Both milling steps were done in polymer containers. More details are reported in refs. [45,57]. Green bodies were uniaxially pre-pressed in a stainless steel die, followed by cold-isostatic pressing for 15 s at 400 MPa.

For grain growth experiments in electric field, the green bodies were pre-sintered in oxygen at 1425 °C for 1 h in a tube furnace (Carbolite Gero GmbH, Neuhausen), resulting in dense fine-grained microstructures (>99% rel density, grain size of  $1.85 \pm 1.01 \mu\text{m}$ ).

For seeded polycrystals, 2 mm thick slices were cut from the pre-sintered polycrystals using a diamond blade, ground, and polished with diamond slurry of  $0.25 \mu\text{m}$ . The polished surface was partially scratched with a  $30 \mu\text{m}$  diamond grinding disc. The scratches formed pores later during the bonding process, indicating the initial interface between single and polycrystal as needed to analyze the growth length (ref. [49], distance between line of pores and the single-crystal interface, see Figure 4). Strontium titanate single crystals with (100) and (111) surface orientation (SurfaceNet GmbH, Rheine, Germany) were placed between two polished and scratched polycrystalline discs, polished side facing to the single crystal, and diffusion-bonded by applying a load of 1 MPa at 1430 °C for 20 min as described in ref. [49]. The obtained seeded polycrystal was cut in 2 mm thick slices perpendicular to the single-crystal interface for field-assisted annealing.

The experimental setup for field-assisted microstructure evolution used platinum sheets as electrodes, plated on thin alumina plates (0.6 mm) to block the electric currents (<10 mA), as shown in Figure 1 and described in detail in refs. [6,7]. The electrodes were at least twice as large as the samples. A small block of alumina ( $\approx 30 \text{ g}$ ) was placed on top of the upper electrode to keep the stack of sample and two electrodes in place. The electrodes were connected with platinum wires to a power source (XG 600-2.8, AMETEK, San Diego, USA). A thin layer of coarse zirconia (Luxfer MEL Technologies, Manchester, UK) was used as a separator to prevent a chemical reaction of alumina and strontium titanate.

The interface of the single crystals was placed parallel to the field.

The heat treatments were done in a tube furnace (Carbolite Gero GmbH, Neuhausen) in air or nitrogen at temperatures between 1350 and 1450 °C for 10 h at nominal electric fields from 50 to  $150 \text{ V mm}^{-1}$  with a heating rate of  $10 \text{ K min}^{-1}$  and a cooling rate of  $10 \text{ K min}^{-1}$ . Due to the 0.6 mm alumina plates separating the sample and the electrode, approximately 43% of the total electric field reached the sample, neglecting the thin layer of zirconia powder.<sup>[6,7]</sup>

After the heat treatment, cross sections along the electric field were cut, ground, and polished with diamond slurry to  $0.25 \mu\text{m}$ , and the microstructure was analyzed by scanning electron microscope (SEM, FEI Nova NanoSEM 450, environmental mode with 0.4 mbar water vapor pressure) from electrode to electrode, as indicated in Figure 1B. The growth length of the single crystals was analyzed graphically on SEM images of the entire growth front of the single crystal. For this procedure, SEM images were taken from the left to the right electrode with some overlap to allow stitching them together. On these images, the growth length was obtained by measuring the distance between the zero line and the actual position of the interface of the single crystal in every pixel of the image. More details of this procedure are given in refs. [6,49].

AC grain growth experiments were done on non-polished 2 mm thick polycrystalline discs in the same experimental setup described earlier, but in a batch furnace (Carbolite Gero GmbH, Neuhausen, Germany) at temperatures between 1350 and 1500 °C with heating times of up to 20 h in air. To generate AC voltages, a bipolar switching circuit was connected between the electrodes and the power source, providing a rectangular voltage profile with frequencies from 0 to  $\frac{1}{4} \text{ Hz}$ . The AC electric field was 50 or  $75 \text{ V mm}^{-1}$  (total).

For all field-assisted grain growth experiments, a field-free sample was present in the same furnace run to provide a benchmark. In some cases, the data from the benchmark samples is presented later.

Grain sizes were analyzed by the line intersection method on SEM images from 10 equally distanced positions between the electrodes, counting typically 30–150 grains per image. Grain sizes above  $80 \mu\text{m}$  must be considered as approximation due to poor counting statistics.

Field-assisted sintering experiments were done using the setup and furnace for the DC experiments in oxygen at 1280 °C, that is, with blocking alumina plates and zirconia powder, for different heating times. Green bodies were slightly below 3 mm thick. A 3 mm thick alumina C-ring was placed around the green bodies and between the electrodes to keep the electric field of nominally

**Table 1.** Summary of all experiments reported in this study.

Experiment type	Crystal orientation	Atmosphere	Temperature [°C]	Frequency [Hz]	Field [V mm <sup>-1</sup> ]
Anisotropy	(100) and (111)	Air	1450	0 (DC)	0, 150
Atmosphere	(100)	N <sub>2</sub>	1350, 1425, 1450	0 (DC)	100
Frequency	Polycrystalline	Air	1350, 1450, 1500	1/4, 1/6, 1/20, 1/40	50, 75
Sintering	Polycrystalline	Air	1280	0 (DC)	0, 200

200 V mm<sup>-1</sup> constant during sintering and to prevent an influence of the mechanical pressure from the electrode and the alumina block used to keep the electrode in place. The samples were cut parallel to the electric field, polished, and analyzed by SEM on 10 equally spaced positions along the center from electrode to electrode. The local porosity was taken from the SEM images.

**Table 1** gives an overview of all experiments conducted in this study.

### 3. Grain Growth in DC Electric Fields in Strontium Titanate: A Short Review

The present study extends previous reports on the impact of electric field on grain growth and sintering in strontium titanate.<sup>[6–8]</sup> As a basis for the discussion in the following sections, this section summarizes the previous studies.

Experiments with seeded polycrystals were used before on various materials including alumina,<sup>[58–60]</sup> barium titanate,<sup>[61,62]</sup> and strontium titanate.<sup>[63–65]</sup> The benefit of such experiments compared to classical experiments is the well-defined driving force for growth of the single crystal, which allows, for example, an evaluation of the anisotropy of the grain-boundary mobility.<sup>[49,65–67]</sup> Here and in previous studies,<sup>[6,7]</sup> this well-defined driving force was used to experimentally access grain growth gradients as apparent after annealing some functional ceramics in electric field. Such gradients are usually referred to as graded microstructure and grain size between the electrodes and are documented for various materials including alumina,<sup>[9,10]</sup> zirconia,<sup>[68]</sup> zinc oxide,<sup>[24,69]</sup> and barium titanate.<sup>[11,70]</sup>

The setup shown in Figure 1 was used to analyze the impact of electric fields on grain growth in oxidizing atmosphere in strontium titanate.<sup>[6,7]</sup> It was found that single-crystalline seeds grow faster into a polycrystalline matrix at the negative electrode compared to the positive electrode (**Figure 2A**). This observation was found to depend on the temperature. Below 1460 °C, very long heating times were required to observe such grain growth gradients in electric field. In general, the grain sizes followed similar gradients as the single-crystalline seeds, that is, faster grain growth at the negative electrode. Growth at the positive electrodes resembles grain growth in the absence of electric fields,<sup>[6]</sup> and growth at the negative electrode is significantly faster than grain growth in the absence of electric field.

For grain growth in the absence of electric fields, reducing atmospheres are known to result in faster grain growth rates for both polycrystals and single-crystalline seeds.<sup>[52]</sup> From this observation, it was hypothesized that the electric field causes a migration of oxygen vacancies toward the negative electrode (**Figure 2B**). At temperatures of 1350 °C and above, oxygen-

vacancy diffusion in strontium titanate is fast enough to reach equilibrium concentration profiles within minutes or even seconds.<sup>[6,7,38]</sup> Cationic defects (strontium vacancies, acceptors, or donors from impurities) have diffusion coefficients which are too low to allow any long-range diffusion in electric field in the time scale used for the present experiments.<sup>[6,7,39,40]</sup>

As the electrodes were blocking electronic currents, no permanent current can flow, and this includes all mobile charge carriers, that is, electrons, holes, and oxygen vacancies. Accordingly, once high temperature is reached and electric fields are present, oxygen vacancies will diffuse toward the negative electrodes similarly to what was observed at lower temperatures (degradation of dielectrics<sup>[71–74]</sup>), and similar equilibrium profiles will be reached. Accordingly, in electric field, the negative electrode is reduced by the accumulation of oxygen vacancies. Faster grain growth is a consequence of the reduction at the negative electrode (**Figure 2B**). It was argued that this faster grain growth in reducing atmosphere in general and at the negative electrode in particular is caused by space charge and solute drag as detailed in the following (refs. [6,7], **Figure 2B–F**).

For strontium titanate, grain-boundary cores are positively charged and bear a negative space-charge layer compensating the core charge (refs. [43,75,76], **Figure 2D**). Detailed understanding is available on how the space-charge layer depends on temperature and oxygen partial pressure.<sup>[7,43,77,78]</sup> Specifically, it is well-known that lower-oxygen partial pressures result in less grain-boundary core charge and less space charge (**Figure 2C**). The space-charge layer refers to accumulation (depletion) profiles for all relevant point defects. In the context of the present study, only cationic defects matter as their low diffusion is limiting grain-boundary migration.

Detailed grain growth investigations have revealed that the space-charge layer impact grain growth.<sup>[6,7,49,50]</sup> The mechanism seems to be similar to solute drag.<sup>[44,78,79]</sup> The cationic point defects at the grain boundary (both in the core and the space-charge layer) exert diffusional drag on grain-boundary motion. Accordingly, less space charge with less cationic segregation results in less diffusional drag and a higher grain-boundary mobility (**Figure 2**), which was observed experimentally both in the absence and in the presence of an electric field.

Accordingly, faster grain growth at the negative electrode occurs because of less cationic segregation in the grain-boundary core and space charge, resulting in less diffusional drag on grain-boundary motion and a higher grain-boundary mobility.

Beyond grain growth in electric field with blocking electrodes, similar gradients in grain size were found after flash sintering: for both undoped and Fe-doped strontium titanate, coarser microstructures were observed at the negative electrode.<sup>[8]</sup> In this case, a transmission electron microscopy, energy-dispersive

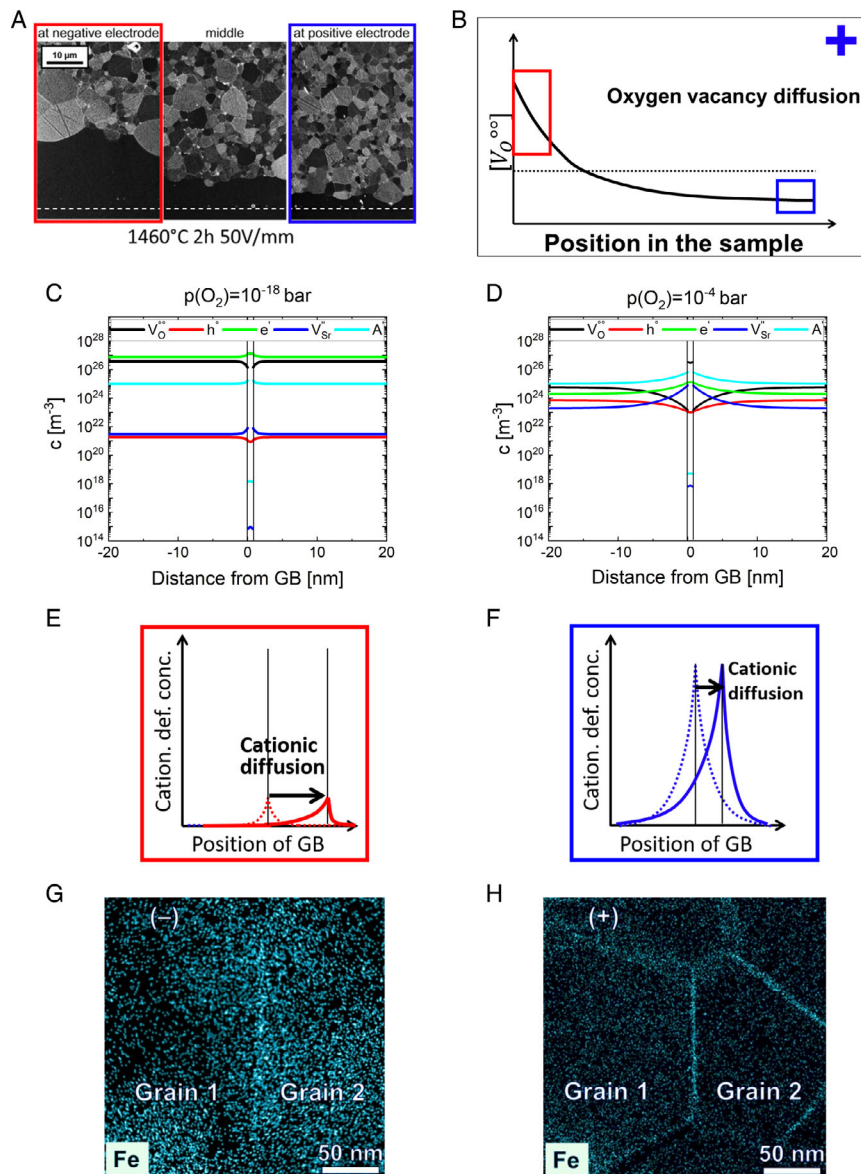


**Figure 2.** A) Growth of single-crystalline seeds into a polycrystalline matrix in electric field. The electric field acted horizontally, that is, along the grain boundary of the single crystal. Faster grain growth at the negative electrode is evident. B) The electric field causes a redistribution of oxygen vacancies, such that the material becomes partially reduced at the negative electrode. Calculated concentration profiles at the grain boundaries in C) reducing and D) oxidizing atmosphere, resulting in E) high and F) low grain-boundary mobility. Acceptor (Fe) dopant concentrations at grain boundaries after flash sintering at the G) negative and H) positive electrode. (B, E, F, G, H) are reproduced with permission from ref. [8]. (C, D) are reproduced with permission from ref. [7]. (A) is reproduced with permission from ref. [6].

X-ray spectroscopy (TEM–EDS) analysis has revealed that less cationic segregation (i.e., Sr vacancies or Fe) occurs at the negative electrode, supporting the argumentation provided earlier (Figure 2).

In addition, a series of studies investigated the impact of electric fields on the atomistic grain-boundary structure,<sup>[13–15]</sup> documenting changes of the grain-boundary atomic and electronic core structure by the electric field. The most recent study documents a higher-oxygen-vacancy concentration at the negative electrode by X-ray photoelectron spectroscopy (XPS) and electron energy loss spectroscopy (ELNES),<sup>[13]</sup> further supporting the oxygen-vacancy migration by the electric field.

## 4. Results and Discussion

### 4.1. Grain Growth in DC Electric Fields: Anisotropy

To analyze the impact of the anisotropy of the grain-boundary mobility, two different surface orientations of the single crystal were analyzed, that is, (100) and (111). Such a setup was used before to characterize the anisotropy of the grain-boundary mobility.<sup>[49,66]</sup> The experiment was done at 1450 °C with 150 V mm<sup>-1</sup> and a heating time of 10 h. The obtained growth length is shown in **Figure 3** and corresponding representative microstructures in **Figure 4**. The field-free benchmark samples

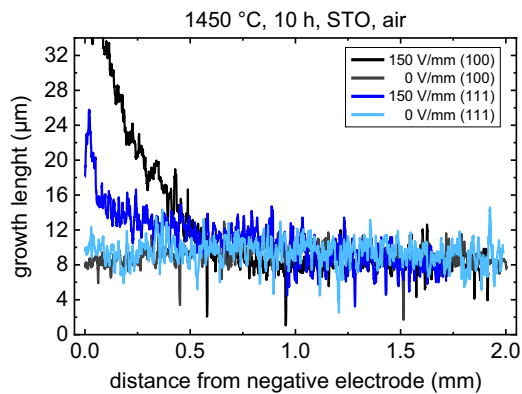


**Figure 3.** Growth of seeded polycrystals heat treated at 1450 °C for 10 h in air in DC electric fields. The (100) orientation shows a more pronounced growth under electric field than the (111) orientation.

show very homogeneous growth and, as expected, the growth of these two orientations is very similar.<sup>[49,66]</sup>

At the negative electrode, the single crystal with (100) orientation shows more growth into the polycrystal than the (111) orientation. The difference amounts to a factor of about two, indicating a difference in the grain-boundary mobility of about  $\sqrt{2}$  due to the parabolic grain growth law.<sup>[49,66]</sup> In addition, the layer of enhanced grain growth reaches further into the center of the sample for the (100) orientation compared to (111). At comparable temperatures and in the absence of electric fields, both orientations have almost the same mobility.<sup>[49,66]</sup> However, the present experiments show that both orientations react differently to the oxygen-vacancy redistribution in electric field: the (100) orientation experiences more increase in the grain-boundary mobility at the negative electrode.

As discussed in Section 3, the negative electrode corresponds to reducing conditions. Accordingly, the findings indicate that the dependence of the grain-boundary mobility on the atmosphere is stronger for the (100) orientation compared to (111).

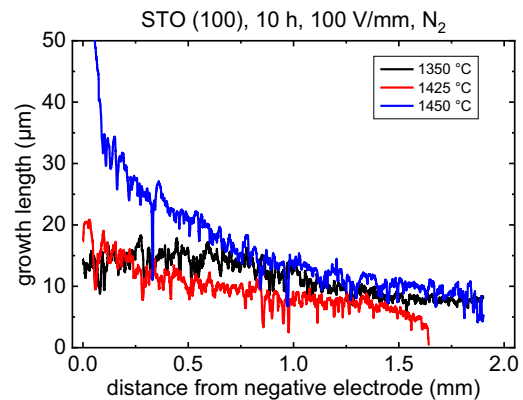


**Figure 5.** Growth lengths of seeded polycrystals with (100) orientation heat-treated for 10 h at different temperatures in nitrogen.

This agrees well with previous observations, where the anisotropy was investigated for different oxygen partial pressures.<sup>[49,66]</sup>

#### 4.2. Grain Growth in DC Electric Fields: Atmosphere

The experiment shown in Figure 1 was done in nitrogen for a (100) orientation to analyze the impact of the oxygen partial pressure. The obtained growth lengths for a heating time of 10 h at 100 V mm<sup>-1</sup> and for three different temperatures are shown in Figure 5. The corresponding microstructures are given in Figure 6. As in oxidizing atmosphere, more growth of the single crystals occurs at the negative electrode. At 1350 °C, the polycrystals show significant coarsening at the negative electrode and at the sample center (Figure 6), similar to the single crystals. At 1425 °C, the growth length at the negative electrode is similar to 1350 °C and decreases from the center toward the positive electrode. At 1450 °C, a much stronger decrease in the growth length from the negative electrode to the positive electrode was obtained. At 1425 and 1350 °C, the polycrystals showed slightly more grain growth at the negative electrode with a tendency to bimodal

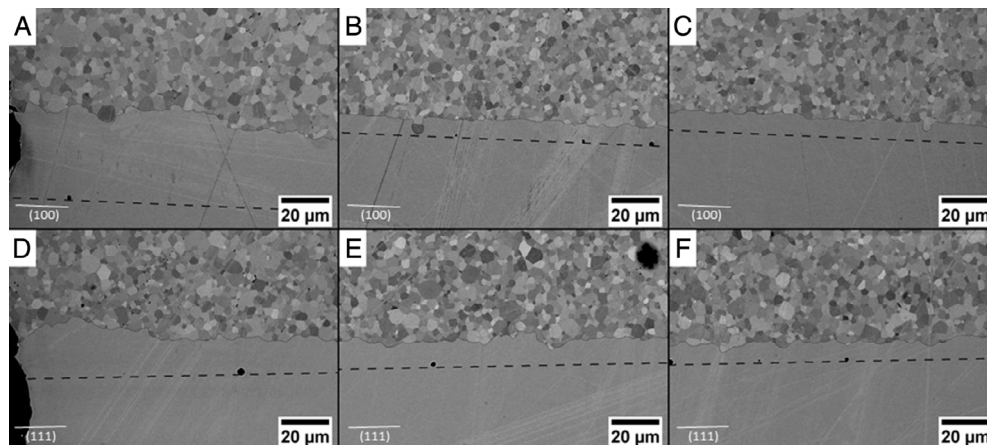


**Figure 4.** Corresponding microstructures for the two samples with field from Figure 3, heat treated for 10 h in air at 1450 °C with 150 V mm<sup>-1</sup> applied. At the bottom are the single crystals, growing into the polycrystals on top. The black dashed line indicates the initial interface between polycrystals and single crystal as marked by a row of small pores. A–C) The (100) single-crystal orientation and D–F) the (111) orientation. Microstructures taken from the (A,D) negative electrode, (B,E) center position, and (C,F) positive electrode. The black area in (E) is caused by surface contamination from preparation.

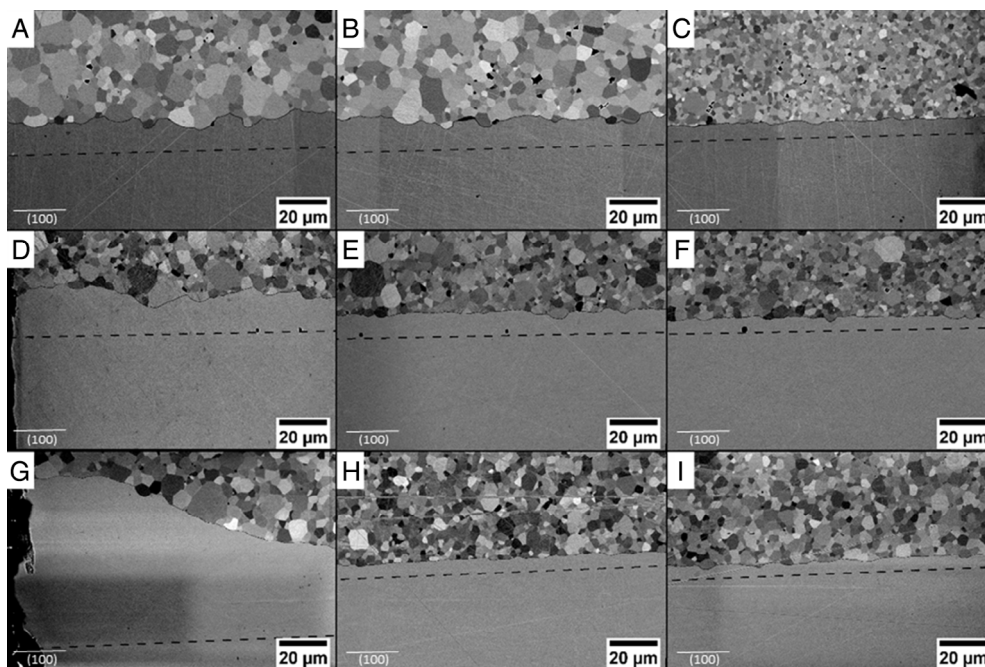


**Figure 6.** Exemplary microstructures of the samples heat-treated for 10 h at different temperatures with  $100 \text{ V mm}^{-1}$  in nitrogen. The lower gray area corresponds to the single crystal growing into the polycrystal. The black dashed line indicates the initial interface between polycrystal and single crystal. A–C) Heated to  $1350 \text{ }^\circ\text{C}$ , D–F) to  $1425 \text{ }^\circ\text{C}$ , and G–I) to  $1450 \text{ }^\circ\text{C}$ . Microstructures were taken from (A, D, G) the negative electrode; (B, E, H) center position; (C, F, I) and positive electrode.

microstructures, as expected for strontium titanate at these temperatures.<sup>[49,51]</sup> All microstructures in nitrogen are slightly coarser than in air.<sup>[6,7]</sup> Slower grain growth at  $1425 \text{ }^\circ\text{C}$  compared to  $1350 \text{ }^\circ\text{C}$  is expected for strontium titanate, where non-Arrhenius grain growth with a local minimum in the grain growth constant at  $1425 \text{ }^\circ\text{C}$  occurs (refs. [46,49–52,80], see Section 4.5).

During the heat treatment in nitrogen, the oxygen partial pressure was lower than in air. Annealing in forming gas (i.e., much lower partial pressure) was reported to cause faster growth in the absence of electric field,<sup>[52]</sup> and following Section 3, the electric field results in a partial reduction at the negative electrode. Apparently, these two effects superpose, resulting in a stronger reduction of the negative electrode and much faster grain growth.

Calculations of the  $p(\text{O}_2)$  dependence of the grain-boundary potential resulted a slightly larger grain-boundary potential for mildly reducing atmospheres (such as nitrogen) than for air.<sup>[7]</sup> As for strontium titanate, grain growth rates seem to be linked to segregation as caused by grain-boundary core charge and space charge, grain growth rates in air and nitrogen should be comparable, which agrees well with the present experiment. At the negative electrode, where grain growth is faster than in air and at the positive electrode, the material becomes reduced enough to impact grain growth. Overall, this observation indicates that the electric field has a stronger impact on the oxidation state of strontium titanate than the atmosphere.

### 4.3. Grain Growth in AC Electric Fields

In addition to DC electric fields, AC electric fields were used to induce an oscillation of oxygen vacancies and evaluate its impact

on grain growth. The relevant frequency range was estimated by using single-crystal diffusion data from the literature. The drift velocity  $\nu_D = \mu E$  with drift velocity  $\nu_D$ , mobility  $\mu$ , and electric field  $E$  was coupled with the Nernst–Einstein relation, coupling mobility to the diffusion coefficient  $D$

$$\nu_D = E \cdot \frac{D \cdot q}{k_B \cdot T} \quad (1)$$

with  $q$  as the charge of the charged species,  $T$  as the temperature, and  $k_B$  as the Boltzmann constant. Considering  $E = 50 \text{ V mm}^{-1}$ ,  $T = 1425 \text{ }^\circ\text{C}$ ,  $q = 2$ , and  $D_{\text{Vo}} = 10^{-5} \text{ cm}^2 \text{ s}^{-1}$ ,<sup>[38]</sup> the drift velocity of oxygen vacancies is approximately  $40 \text{ mm min}^{-1}$  and the time  $t_{2\text{mm}}$  to diffuse 2 mm is about 3 s (corresponding to a frequency of 1/6 Hz). This approximation is ignoring grain boundaries, which lower the overall diffusion coefficient and result in longer diffusion times (and lower frequencies) across 2 mm. Based on this approximation, AC frequencies were chosen as 0.25, 0.166, 0.05, and 0.025 Hz. The intention was to select frequencies above and below the estimated diffusion time, such that two different cases should occur: one where the frequency is too high such that the oxygen-vacancy migration does not span the entire sample, and one where it does span the entire sample and accumulation effects of oxygen vacancies at the electrode should occur.

For AC electric fields, only polycrystals were evaluated. The mean grain sizes for different temperatures and 10 h heating time are shown in Figure 7. At 1/6 Hz, an additional measurement was done with a higher electric field, that is,  $75 \text{ V mm}^{-1}$ . For  $1350 \text{ }^\circ\text{C}$  (Figure 7A), no significantly increased grain growth was found anywhere in the sample, regardless of the applied frequency and field. At this temperature, grain growth acceleration

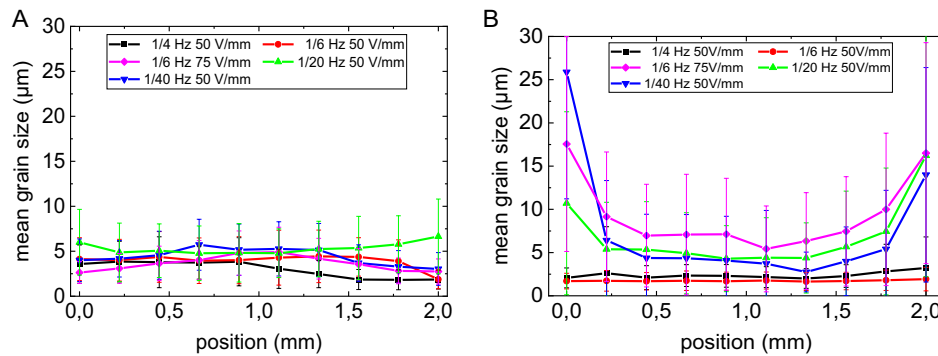


**Figure 7.** Mean grain sizes for samples heat-treated at A) 1350 °C and B) 1450 °C for 10 h at 50 V mm<sup>-1</sup> with different AC frequencies. At 1350 °C, there is no effect of the AC field on grain growth. At 1450 °C and lower frequencies (B), much faster growth could be observed at both electrodes. At 1450 °C, an increase of the field to 75 V mm<sup>-1</sup> at 1/6 Hz resulted in much faster grain growth as well.

at the negative electrode of DC electric fields was reported to be moderate<sup>[6,7]</sup> and the drift velocity of oxygen vacancies is lower than the approximation from the aforementioned; accordingly, this behavior is expected. At 1450 °C (Figure 7B), a layer with enhanced grain growth was found near both electrodes for low-enough frequencies, that is, 1/20 Hz and 1/40 Hz at 50 V mm<sup>-1</sup>. At 1/6 Hz, a higher field strength of 75 V mm<sup>-1</sup> also resulted in faster grain growth at the electrodes.

Representative microstructures corresponding to Figure 7 are displayed in Figure 8. For 1350 °C, a homogeneous microstructure appears throughout the sample after 10 h at 50 V mm<sup>-1</sup> with 1/20 Hz (Figure 8A–C), which is expected from Figure 7. At 1450 °C (Figure 8D–F), bimodal microstructures are evident with more large grains in the vicinity of the electrodes. This feature is discussed in detail in Section 4.5.

For DC electric fields, enhanced grain growth was observed at the negative electrode, if the temperatures were high enough. The effect was understood by a redistribution and accumulation

of oxygen vacancies at the negative electrode (see Section 3). These observations can be applied to grain growth in AC electric field: according to Figure 7 and 8, AC electric fields cause faster grain growth at both electrodes at high temperatures and low frequencies. Apparently, both electrodes are reduced during the experiment. There are two possible explanations for this reduction.

The first one is an electromigration of oxygen vacancies in the electric field, similar to the observations in DC electric field. As discussed with Equation (1), the drift velocity of oxygen vacancies in electric field is high enough to allow a diffusion across the entire sample in the time scale provided by the frequency of the AC field. Accordingly, if the frequency is low enough, the existing oxygen vacancies are moved toward the currently negative electrode for some time, resulting in a temporary local reduction. When the polarity is reversed, the oxygen vacancies migrate to the other electrode, resulting in a temporary local reduction there. Accordingly, both electrodes become reduced temporary.

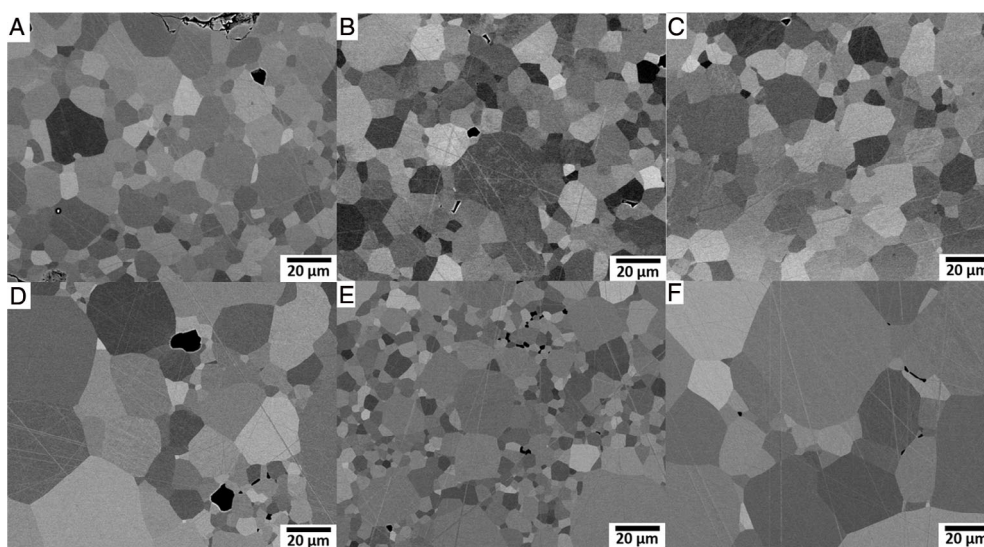


**Figure 8.** Exemplary microstructures of AC experiments at different temperatures, 10 h, 50 V mm<sup>-1</sup>, and 1/20 Hz at A–C) 1350 °C and D–F) 1450 °C. Images taken at the (A, D) top and (C, F) bottom electrode and at (B, E) the sample center.

In the same way as discussed in Section 3, the reduction results in faster grain growth. Note that this explanation agrees with the observed coarser microstructures in the center of the sample (see Figure 7), as the oxygen vacancies are migrating back and forth through the center, likely similar to a reduction front.<sup>[12,71–74]</sup> As this electromigration takes time, a threshold frequency should exist. As evident in Figure 7, this threshold is between  $1/6$  and  $1/20$  Hz, which agrees well with the approximation given earlier, where  $1/6$  Hz was predicted for 1425 °C along with the expectation of the true frequencies being somewhat lower.

The other possible explanation is a reduction of the surface layers at the anode by a loss of oxygen to the atmosphere, as the temperature was high and the electrodes were not blocking oxygen. The oxygen ions might be driven out of the lattice at the positive electrode, forming oxygen molecules in the atmosphere



This would occur on both electrodes alternately as the polarity changes, and is only relevant if the incorporation of oxygen at the cathode (i.e., the oxidation reaction) is slower than the reduction reaction at the anode, for example, for kinetic reasons or catalytic effects at the surfaces. However, it is not clear if this premise holds. In addition, it is not clear why such a reduction should depend on the frequency of the AC electric field. Accordingly, while certainly possible, this effect can be assumed to be of minor importance or even negligible, and we assume that the electromigration of oxygen vacancies is causing the local reduction.

Note that in all cases with enhanced grain growth at the electrodes, a coarser microstructure was observed in the sample center compared to samples without enhanced grain growth at the electrode. In some cases, the increase in grain size was more than a factor of 2. Generally, this observation agrees with both of the possible explanations. If an electromigration of oxygen vacancies causes faster grain growth at both electrodes, every polarity reversal induces a wave of oxygen vacancies migrating from one electrode to the other. While this wave passes through the center of the sample, it causes faster grain growth there. If a reduction occurs at both electrodes by a loss of oxygen to the surface, this reduction could reach inward to the center of the sample, causing faster grain growth.

In contrast to the observations at 1450 °C shown in Figure 7B, a complete grain growth stagnation was observed at 1500 °C in AC electric field. This is evident in Figure 9A for different heating times and in Figure 9B for different frequencies. Representative microstructures are depicted in Figure 10. This behavior is completely unexpected as at this temperature, the drift velocity of oxygen vacancies is certainly high enough for an electromigration in electric field, and grain growth is known to be very fast in the absence of electric field at this temperature.<sup>[46,51]</sup> Without electric field, mean grain sizes typically reach more than 20 μm within a few hours. In DC grain growth experiments at similar temperatures, no grain growth stagnation, but a clear increase of grain growth rates at the negative electrode by the electric field was observed.<sup>[6,7]</sup> Note that these studies used the same powder processing and the same furnaces in the same lab as this study and, thus, the results are well comparable.

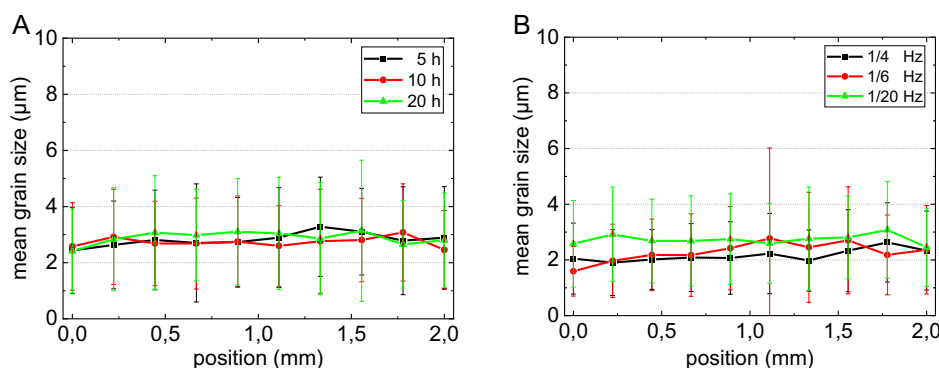


**Figure 9.** A) Mean grain sizes for different heating times at 1500 °C, 50 V mm<sup>-1</sup>, and  $1/20$  Hz. B) Mean grain sizes for different frequencies at 1500 °C with 10 h heating time and 50 V mm<sup>-1</sup>.

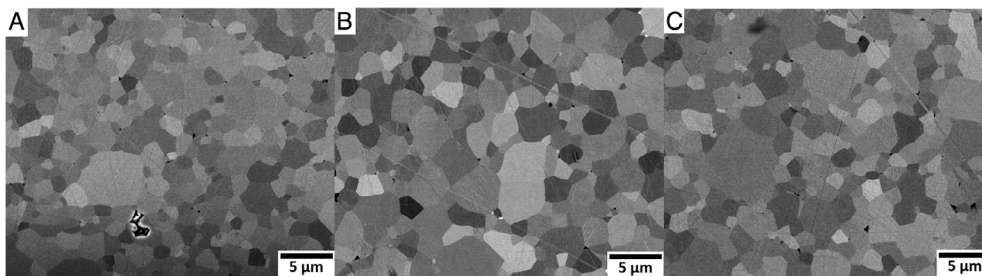


**Figure 10.** Microstructures after heating to 1500 °C for 10 h with 50 V mm<sup>-1</sup> at  $1/6$  Hz at the A) top, B) center, and C) bottom of the specimen.

The underlying mechanism is unclear. For strontium titanate, grain growth stagnation is known to occur (but for much larger grain sizes) and was related to a solute drag-like mechanism by the cationic defects accumulated in the space-charge layer and the grain-boundary core.<sup>[49–51]</sup> For barium titanate, grain-boundary faceting and nucleation barriers for grain-boundary migration were identified to be relevant.<sup>[61,62,81]</sup> In either case, it is not clear why an AC electric field (and not a DC electric field) causes this stagnation.

Still, this is a drastic observation with potential use for applications: stabilizing fine-grained microstructures at high temperatures is sometimes highly desired to assure optimal properties. So far, no method is known to stabilize grain sizes below 4  $\mu\text{m}$  at temperatures above 1450  $^{\circ}\text{C}$  in strontium titanate. It is to be investigated if similar grain growth stagnation by AC electric field occurs in similar materials, for example, other perovskites or functional ceramics.

## 5. Sintering in DC Electric Fields

In addition to field-assisted grain growth experiments, sintering was investigated in DC electric field with blocking electrodes. The locally resolved pore fraction for different heating times at 1280  $^{\circ}\text{C}$  is shown in **Figure 11**. For short heating times and enough remaining porosity ( $>5\%$ ), the field-assisted samples have a slightly lower porosity and, accordingly, slightly faster sintering. No gradient in porosity from one electrode to the other is visible. This difference in porosity is lost for longer heating times above 4 h when the density increases to above 95%.

The observed field effect differs from the effect on grain growth in ceramics discussed earlier, as the field accelerates shrinkage homogeneously while the grain growth is accelerated locally. The effect also occurs at temperatures well below the threshold at which the field-driven grain growth acceleration in dense strontium titanate was reported, that is, above 1350  $^{\circ}\text{C}$ .<sup>[5]</sup>

Few reports discuss a direct impact of electric fields on sintering mechanisms (i.e., excluding thermal effects by electric currents). One similar study reports enhanced surface diffusion during sintering in a non-contacting field for Mg–Al spinel.<sup>[62]</sup>

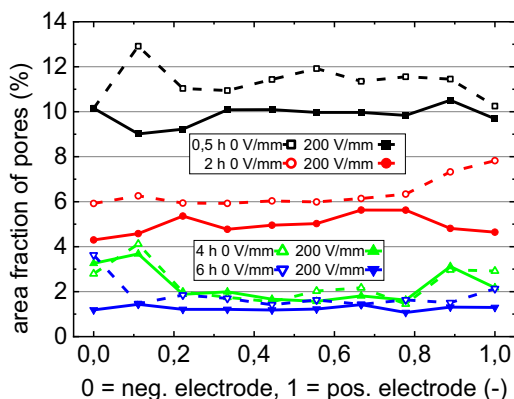


**Figure 11.** Pore fractions of green bodies sintered in an external electric field. The dashed lines correspond to field-free sintering, the solid lines to the sintering in DC electric field. Sintering was done in oxygen at 1280  $^{\circ}\text{C}$  and 200  $\text{V mm}^{-1}$  for different heating times.

In a recent series of studies on Y-doped ceria, intermediate-stage sintering was found to be changed by AC electric fields.<sup>[20,82–84]</sup> In these studies, the electric field was found to change many parameters, including the activation energy for sintering, the sintering stress and the viscosity during sintering. While the change of these parameters is well documented, the physical reason behind these changes is not fully understood. In the present case, the change in densification in Figure 11 points in a similar direction as for Y-doped ceria. However, more elaborated sintering experiments are needed to compare the details and to further investigate the fundamentals of the effect of electric fields on sintering.

### 5.1. Field-Assisted Grain-Boundary Transitions

Electrochemical grain-boundary transitions are known theoretically<sup>[85]</sup> and experimentally.<sup>[86]</sup> For strontium titanate, Section 3 has discussed the importance of defect chemistry for grain-boundary migration in electrochemical context, that is, in the presence of electric fields.

In the absence of electric fields, strontium titanate is known for the occurrence of grain-boundary transitions,<sup>[46,49–52,80]</sup> resulting in non-Arrhenius grain growth: below 1350  $^{\circ}\text{C}$ , grain growth rates follow classical Arrhenius behavior. From 1350  $^{\circ}\text{C}$ , growth rates decrease by orders of magnitude to 1425  $^{\circ}\text{C}$  and then increase again, showing again Arrhenius behavior. In addition, from 1350  $^{\circ}\text{C}$ , microstructures are bimodal. Overall, this phenomenon is likely caused by the existence (and coexistence) of two grain-boundary types with different grain-boundary mobility<sup>[46,49,51,66]</sup> and energy.<sup>[80]</sup> Despite intense TEM investigation, no difference of the grain-boundary structure could be found for these two types.<sup>[53–56]</sup> However, there seem to be chemical changes: in bimodal microstructures, grain boundaries of small grains tend to be Ti rich, while large grains tend to have stoichiometric boundaries or even Sr excess.<sup>[87,88]</sup> It must be pointed out that these TEM observations are a trend only due to low statistics. However, overall, this points toward the two different grain-boundary types being related to the cationic concentration profile of grain boundaries, that is, both the grain-boundary core and the space-charge layer. The slow grain boundaries would be the ones with space charge, while the fast boundaries have less space charge.<sup>[7,49,50]</sup> As transition between these two types, break-away events from the space-charge layer were suggested<sup>[44,78]</sup> as predicted by the solute drag model.<sup>[79,89,90]</sup>

In the present and preceding studies,<sup>[6–8]</sup> the role of space charge and cationic segregation on grain-boundary migration in strontium titanate has been understood in a degree of detail that is unique among functional ceramics. In addition to this knowledge, the electric field impacts the bimodality of microstructures: the faster grain growth of polycrystals at the electrodes in AC or DC electric fields always results in bimodal microstructures, with the grain size being dominated by the large grains. This is obvious, for example, in Figure 7. Bimodal microstructures in strontium titanate are a consequence of the coexistence of two grain-boundary types. As such, it seems that the presence of the electric field is impacting the transition between the two grain-boundary types. Likely, this impact is indirect

(similar to what was discussed in Section 3), that is, not by the electric field itself, but by the local oxygen-vacancy concentration and the resulting grain-boundary properties. This agrees well with previous findings, where the oxygen partial pressure was found to impact the Arrhenius behavior of grain growth in the absence of electric fields.<sup>[52]</sup>

Of particular interest is the observation of almost complete grain growth stagnation at 1500 °C in AC electric fields. While this effect cannot be understood based on the present findings, it does indicate that these conditions suppress a grain-boundary transition to the fast type. It is to be investigated if such effects occur in other materials where excessive and bimodal grain growth is problematic for the application, particularly for dielectric materials based on barium strontium titanate or electrolyte layers for oxygen-, hydrogen-, and lithium-based applications.

Overall, the present experiments indicate that electric fields can cause grain-boundary transitions in strontium titanate, similar to what was observed in other materials.<sup>[85,86]</sup>

## 6. Summary and Conclusions

The present study investigates the impact of weak electric fields, both AC and DC, on microstructure evolution in strontium titanate. All experiments used current-blocking electrodes to prevent Joule heating. An overview of all experiments is given in Table 1. This study extends previous results, which focused on the impact of DC electric fields on grain growth.<sup>[6–8]</sup> From previous experiments, it is known that the electric field results in a migration of oxygen vacancies toward the negative electrode, where a local reduction causes a decrease in space charge and cationic segregation and, in turn, a higher grain-boundary mobility. Overall, the present study confirms these findings.

For DC experiments, seeded polycrystals were chosen, as this setup provides a well-defined driving force. The setup was used to investigate the impact of electric fields on grain growth and sintering, where the focus was on the crystal orientation and the atmosphere. The impact of DC electric fields was found to be stronger for the (100) orientation compared to (111), indicating that the impact of the oxygen vacancies on the grain-boundary mobility depends on the grain-boundary orientation. When reducing atmospheres are used during the application of DC electric fields, very strong gradients in grain growth become evident, again underlining the interpretation of an oxygen-vacancy migration causing the change in grain growth behavior.

In AC electric fields at 1450 °C, grain growth in polycrystalline specimens was significantly faster on both electrodes, if the frequency was low enough. Approximating the drift velocity of oxygen vacancies, these results could be understood in a temporary reduction of the regions near the electrodes: the AC electric field causes an oscillation of the oxygen vacancies between the two electrodes. If the frequency is low enough, the oxygen vacancies accumulate in both electrode regions alternately, causing faster grain growth. If the frequency is too high, there is insufficient time for the oxygen vacancies to accumulate at both electrodes, such that no effect on grain growth becomes visible.

However, at higher temperatures (1500 °C), applying an AC electric field resulted in a complete grain growth stagnation at

very low grain sizes. This is unexpected as both in the absence of electric fields and with DC electric fields, fast grain growth was observed. The mechanism behind this effect is not clear. However, it is technologically relevant: limiting grain growth is of central interest for many applications, and potentially, this effect exists in other materials as well, for example, barium strontium titanate.

A simple analysis of grain growth in non-contacting electric field has revealed that sintering is slightly enhanced for intermediate-stage sintering, which agrees well with the literature.

The findings were used to discuss the impact of electric fields on grain-boundary transitions in strontium titanate. As in previous studies, it is found that the electric field has a similar impact on grain growth at the negative electrode as the oxygen partial pressure in the absence of electric field. Overall, this and three preceding studies<sup>[6–8]</sup> have resulted in a mechanistic understanding of the impact of point defects, segregation and space charge on grain growth in strontium titanate. The detail of this understanding is unique among functional ceramics and can serve as a base to understand more complex functional ceramics particularly in the group of perovskites. Beyond extending our fundamental understanding of grain growth, this study demonstrates that electric fields can be used as a tool of controlling grain growth. Both faster and slower grain growth can be achieved, depending on the selection of parameters.

## Acknowledgements

The work was supported by the German Research Foundation (DFG) under (grant nos. HO 1165/20-1 and HO 1165/22-1) within the priority program SPP 1959, and under the Emmy-Noether-Program (grant no. RH 146/1).

Open Access funding enabled and organized by Projekt DEAL.

## Conflict of Interest

The authors filed a patent on grain growth stagnation in AC electric fields in ceramics.

## Data Availability Statement

The data that support the findings of this study are available from the corresponding author upon reasonable request.

## Keywords

field-assisted sintering, grain growth, solute drag, space charge

Received: December 20, 2022

Revised: February 27, 2023

Published online:

- [1] O. Guillon, J. Gonzalez-Julian, B. Dargatz, T. Kessel, G. Schierning, J. Räthel, M. Herrmann, *Adv. Eng. Mater.* **2014**, *16*, 830.
- [2] M. Tokita, in *Handbook of Advanced Ceramics: Materials, Applications, Processing, and Properties*, 2nd ed. (Ed: S. Somiya), Academic Press, London; Oxford; Boston; New York; San Diego **2013**, pp. 1149–1177.

- [3] M. Omori, *Mater. Sci. Eng. A Struct. Mater. Prop. Microstruct. Process.* **2000**, 287, 183.
- [4] R. K. Bordia, S.-J. L. Kang, E. A. Olevsky, *J. Am. Ceram. Soc.* **2017**, 100, 2314.
- [5] M. Biesuz, V. M. Sglavo, *J. Eur. Ceram. Soc.* **2019**, 39, 115.
- [6] W. Rheinheimer, M. Fülling, M. J. Hoffmann, *J. Eur. Ceram. Soc.* **2016**, 36, 2773.
- [7] W. Rheinheimer, J. P. Parras, J.-H. Preusker, R. A. D. Souza, M. J. Hoffmann, *J. Am. Ceram. Soc.* **2019**, 102, 3779.
- [8] W. Rheinheimer, X. L. Phuah, H. Wang, F. Lemke, M. J. Hoffmann, H. Wang, *Acta Mater.* **2019**, 165, 398.
- [9] J. I. Choi, J. H. Han, D. Y. Kim, *J. Am. Ceram. Soc.* **2003**, 86, 347.
- [10] J. W. Jeong, J. H. Han, D. Y. Kim, *J. Am. Ceram. Soc.* **2000**, 83, 915.
- [11] H. R. Jin, S. H. Yoon, J. H. Lee, J. H. Lee, N. M. Hwang, D. Y. Kim, J. H. Han, *J. Am. Ceram. Soc.* **2004**, 87, 1747.
- [12] Y. H. Dong, H. R. Wang, I. W. Chen, *J. Am. Ceram. Soc.* **2017**, 100, 876.
- [13] B. Qu, D. Eiteneer, L. A. Hughes, J.-H. Preusker, J. Wood, W. Rheinheimer, M. J. Hoffmann, K. van Benthem, *J. Eur. Ceram. Soc.* **2022**, 4, 1625.
- [14] L. A. Hughes, K. van Benthem, *J. Am. Ceram. Soc.* **2019**, 102, 4502.
- [15] L. A. Hughes, M. Marple, K. van Benthem, *Appl. Phys. Lett.* **2018**, 113, 041604.
- [16] H. Conrad, D. Yang, *Mater. Sci. Eng. A Struct. Mater. Prop. Microstruct. Process.* **2013**, 559, 591.
- [17] H. Majidi, K. van Benthem, *Phys. Rev. Lett.* **2015**, 114, 195503.
- [18] K. Chen, Y. Jiao, Y. Zhao, Y. Gao, X. Zhang, L. An, *Ceram. Int.* **2017**, 43, 12343.
- [19] W. Ji, J. Zhang, W. Wang, Z. Fu, R. Todd, *J. Eur. Ceram. Soc.* **2020**, 40, 5829.
- [20] O. Guillon, R. A. De Souza, T. P. Mishra, W. Rheinheimer, *MRS Bull.* **2021**, 46, 52.
- [21] A. R. Genreith-Schriever, R. A. De Souza, *Phys. Rev. B* **2016**, 94, 224304.
- [22] B. Reeja-Jayan, J. Luo, *MRS Bull.* **2021**, 46, 26.
- [23] S. L. Zhang, H. Q. Wang, M. Y. Lu, C. X. Li, C. J. Li, S. A. Barnett, *J. Power Sources* **2019**, 426, 233.
- [24] X. L. Phuah, W. Rheinheimer, Akriti, L. Dou, H. Wang, *Scr. Mater.* **2021**, 195, 113719.
- [25] T. P. Mishra, R. R. I. Neto, R. Raj, O. Guillon, M. Bram, *Acta Mater.* **2020**, 189, 145.
- [26] S. K. Sistla, T. P. Mishra, Y. Deng, A. Kaletsch, M. Bram, C. Broeckmann, *J. Am. Ceram. Soc.* **2021**, 104, 1978.
- [27] B. Yang, Z. Shang, J. Li, X. L. Phuah, J. Cho, H. Wang, X. Zhang, *J. Eur. Ceram. Soc.* **2022**, 42, 6040.
- [28] H. Wang, X. L. Phuah, H. Charalambous, S. K. Jha, J. Li, T. Tsakalakos, X. Zhang, H. Wang, *Materialia* **2019**, 8, 100451.
- [29] S. K. Jha, K. Terauds, J.-M. Lebrun, R. Raj, *J. Ceram. Soc. Jpn.* **2016**, 124, 283.
- [30] S.-W. Kim, S. G. Kim, J.-I. Jung, S.-J. L. Kang, I.-W. Chen, *J. Am. Ceram. Soc.* **2011**, 94, 4231.
- [31] W. Qin, H. Majidi, J. Yun, K. van Benthem, *J. Am. Ceram. Soc.* **2016**, 99, 2253.
- [32] W. Qin, J. Yun, A. M. Thron, K. van Benthem, *Mater. Manuf. Processes* **2017**, 32, 549.
- [33] F. Lemke, W. Rheinheimer, M. J. Hoffmann, *Scr. Mater.* **2017**, 130, 187.
- [34] R. Moos, K. Härdtl, *J. Am. Ceram. Soc.* **1997**, 80, 2549.
- [35] R. Meyer, R. Waser, J. Helmbold, G. Borchardt, *J. Electroceram.* **2002**, 9, 103.
- [36] R. Meyer, R. Waser, J. Helmbold, G. Borchardt, *Phys. Rev. Lett.* **2003**, 90, 105901.
- [37] R. A. De Souza, V. Metlenko, D. Park, T. E. Weirich, *Phys. Rev. B* **2012**, 85, 174109.
- [38] R. A. De Souza, *Adv. Funct. Mater.* **2015**, 25, 6326.
- [39] K. Gömann, G. Borchardt, M. Schulz, A. Gömann, W. Maus-Friedrichs, B. Lesage, O. Kaitasov, S. Hoffmann-Eifert, T. Schneller, *Phys. Chem. Chem. Phys.* **2005**, 7, 2053.
- [40] K. Gömann, G. Borchardt, A. Gunhold, W. Maus-Friedrichs, H. Baumann, *Phys. Chem. Chem. Phys.* **2004**, 6, 3639.
- [41] R. A. D. Souza, E. C. Dickey, *Philos. Trans. R. Soc. A Math. Phys. Eng. Sci.* **2019**, 377, 20180430.
- [42] F. Gunkel, R. Waser, A. H. H. Ramadan, R. A. De Souza, S. Hoffmann-Eifert, R. Dittmann, *Phys. Rev. B* **2016**, 93, 245431.
- [43] R. A. De Souza, *Phys. Chem. Chem. Phys.* **2009**, 11, 9939.
- [44] K. S. N. Vikrant, W. Rheinheimer, R. E. García, *npj Comput. Mater.* **2020**, 6, 165.
- [45] M. Bäurer, D. Weygand, P. Gumbsch, M. J. Hoffmann, *Scr. Mater.* **2009**, 61, 584.
- [46] W. Rheinheimer, M. J. Hoffmann, *Scr. Mater.* **2015**, 101, 68.
- [47] W. Rheinheimer, M. Hoffmann, *J. Mater. Sci.* **2016**, 51, 1756.
- [48] M. P. Zahler, S. M. Kraschewski, H. Störmer, D. Gerthsen, M. Bäurer, W. Rheinheimer, *J. Eur. Ceram. Soc.* **2023**, 43, 1613.
- [49] W. Rheinheimer, M. Bäurer, C. Handwerker, J. Blendell, M. Hoffmann, *Acta Mater.* **2015**, 95, 111.
- [50] W. Rheinheimer, M. J. Hoffmann, *Curr. Opin. Solid State Mater. Sci.* **2016**, 20, 286.
- [51] W. Rheinheimer, E. Schoof, M. Selzer, B. Nestler, M. J. Hoffmann, *Acta Mater.* **2019**, 174, 105.
- [52] W. Rheinheimer, M. Bäurer, M. Hoffmann, *Acta Mater.* **2015**, 101, 80.
- [53] H. Sternlicht, W. Rheinheimer, M. J. Hoffmann, W. D. Kaplan, *J. Mater. Sci.* **2015**, 51, 467.
- [54] H. Sternlicht, W. Rheinheimer, A. Mehlmann, A. Rothschild, M. J. Hoffmann, W. D. Kaplan, *Scr. Mater.* **2020**, 188, 206.
- [55] H. Sternlicht, W. Rheinheimer, J. Kim, E. Liberti, A. I. Kirkland, M. J. Hoffmann, W. D. Kaplan, *J. Mater. Sci.* **2019**, 54, 3710.
- [56] H. Sternlicht, W. Rheinheimer, R. E. Dunin-Borkowski, M. J. Hoffmann, W. D. Kaplan, *J. Mater. Sci.* **2019**, 54, 3694.
- [57] F. Lemke, W. Rheinheimer, M. Hoffmann, *J. Ceram. Soc. Jpn.* **2016**, 124, 346.
- [58] J. Rödel, A. M. Glaeser, in *Sintering of Advanced Ceramics* (Eds: C. A. Handwerker, J. E. Blendell, W. Kaysser), Vol. 7 of *Ceramic Transactions*, American Ceramic Society, Westerville, OH **1990**, pp. 243–257.
- [59] Y. Finkelstein, S. M. Wiederhorn, B. J. Hockey, C. A. Handwerker, J. E. Blendell, in *Sintering of Advanced Ceramics* (Eds: C. Handwerker, J. Blendell, W. Kaysser), Vol. 7 of *Ceramic Transactions*, American Ceramic Society **1990**, pp. 258–279.
- [60] C. A. Handwerker, P. A. Morris, R. L. Coble, *J. Am. Ceram. Soc.* **1989**, 72, 130.
- [61] M.-G. Lee, S.-M. An, S.-H. Jung, S.-J. L. Kang, *J. Asian Ceram. Soc.* **2013**, 1, 95.
- [62] S.-M. An, B.-K. Yoon, S.-Y. Chung, S.-J. L. Kang, *Acta Mater.* **2012**, 60, 4531.
- [63] S.-Y. Chung, S.-J. L. Kang, *J. Am. Ceram. Soc.* **2000**, 83, 2828.
- [64] S.-Y. Chung, S.-J. L. Kang, *J. Am. Ceram. Soc.* **2002**, 85, 2805.
- [65] W. Rheinheimer, M. Bäurer, H. Chien, G. S. Rohrer, C. A. Handwerker, J. E. Blendell, M. J. Hoffmann, *Acta Mater.* **2015**, 82, 32.
- [66] W. Rheinheimer, J. E. Blendell, C. A. Handwerker, *Acta Mater.* **2020**, 191, 101.
- [67] J. Rödel, A. M. Glaeser, *J. Am. Ceram. Soc.* **1990**, 73, 3292.
- [68] Y. H. Dong, I. W. Chen, *J. Am. Ceram. Soc.* **2018**, 101, 1058.
- [69] X. L. Phuah, J. Cho, Akriti, L. Dou, W. Rheinheimer, R. E. García, X. Zhang, H. Wang, *Nanotechnology* **2020**, 32, 095603.
- [70] H. R. Jin, S. H. Yoon, J. H. Lee, N. M. Hwang, D. Y. Kim, J. H. Han, *J. Mater. Sci. Mater. Electron.* **2005**, 16, 749.
- [71] R. Waser, T. Baiatu, K.-H. Härdtl, *J. Am. Ceram. Soc.* **1990**, 73, 1645.

- [72] R. Waser, T. Baiatu, K.-H. Härdtl, *J. Am. Ceram. Soc.* **1990**, *73*, 1654.  
 [73] R. Waser, T. Baiatu, K.-H. Härdtl, *J. Am. Ceram. Soc.* **1990**, *73*, 1663.  
 [74] J. J. Wang, H. B. Huang, T. J. M. Bayer, A. Moballeggh, Y. Cao, A. Klein, E. C. Dickey, D. L. Irving, C. A. Randall, L. Q. Chen, *Acta Mater.* **2016**, *108*, 229.  
 [75] L. Chick, L. Pederson, G. Maupin, J. Bates, L. Thomas, G. Exarhos, *Mater. Lett.* **1990**, *10*, 6.  
 [76] Y.-M. Chiang, T. Takagi, *J. Am. Ceram. Soc.* **1990**, *73*, 3278.  
 [77] D. S. Mebane, R. A. De Souza, *Energy Environ. Sci.* **2015**, *8*, 2935.  
 [78] K. Vikrant, W. Rheinheimer, H. Sternlicht, M. Bäurer, R. E. García, *Acta Mater.* **2020**, *200*, 727.  
 [79] J. W. Cahn, *Acta Metall.* **1962**, *10*, 789.  
 [80] M. N. Kelly, W. Rheinheimer, M. J. Hoffmann, G. S. Rohrer, *Acta Mater.* **2018**, *149*, 11.  
 [81] J. G. Fisher, S.-J. L. Kang, *Mater. Sci. Forum* **2012**, 715–716, 719.  
 [82] C. Cao, Y. Sasaki, R. Mücke, K. Morita, O. Guillon, *Scr. Mater.* **2020**, *187*, 137.  
 [83] C. Cao, R. Muecke, O. Guillon, *Acta Mater.* **2020**, *182*, 77.  
 [84] C. Cao, R. Muecke, F. Wakai, O. Guillon, *Scr. Mater.* **2020**, *178*, 240.  
 [85] K. S. N. Vikrant, R. E. Garcia, *npj Comput. Mater.* **2019**, *5*, 24.  
 [86] J. Nie, C. Hu, Q. Yan, J. Luo, *Nat. Commun.* **2021**, *12*, 2374.  
 [87] S.-J. Shih, S. Lozano-Perez, D. J. H. Cockayne, *J. Mater. Res.* **2010**, *25*, 260.  
 [88] M. Bäurer, S.-J. Shih, C. Bishop, M. P. Harmer, D. Cockayne, M. J. Hoffmann, *Acta Mater.* **2010**, *58*, 290.  
 [89] K. Lücke, K. Detert, *Acta Metall.* **1957**, *5*, 628.  
 [90] R. Kirchheim, *Acta Mater.* **2002**, *50*, 413.